Effects of radiation heat loss on planar and spherical hydrofluorocarbon/air flames

Justin K. Tavares[a], Vyaas Gururajan[b], Jagannath Jayachandran[a*]

[a]*Aerospace Engineering, Worcester Polytechnic Institute, 100 Institute Rd, Worcester, MA 01609, USA*
[b]*Argonne National Laboratory, 9700 S. Cass Ave., Lemont, IL 60439, USA*

Abstract:
Hydrofluorocarbons (HFC), which are mildly flammable and pose potential fire risks, have received greater attention as a viable low global warming potential alternative to traditional refrigerant and fire-suppressant compounds. Therefore, there is a demand to accurately quantify their flammability and reactivity to establish proper safety metrics. This study investigates the effects of radiation heat loss on slowly-propagating HFC/air laminar flames. Planar 1-D simulations of R-32/air and R-1234yf/air flames show significant reductions in laminar flame speed due to radiative heat losses from the flame zone. Simulations of spherically expanding flames (SEF) revealed that the radiation-induced flow needs to be considered when interpreting data from experiments. To this end, a Spherical-flame RADiation-Induced Flow (SRADIF) model was developed to estimate the burned gas inward flow velocities in constant-pressure SEFs, utilizing the optically thin limit assumption to model radiation heat loss. The model was validated against results from detailed numerical simulations of SEFs, from which radiation-induced inward flow was derived using a new formulation considering both the radiation heat loss and convective flow effects. Results show that SRADIF accurately predicts the inward flow velocity for R-32/air mixtures over a range of conditions and performs significantly better compared to existing analytical models. However, the model was unable to accurately predict flow velocities for R-1234yf/air flames and the reason for this is discussed. (224 words)

Keywords: Hydrofluorocarbons, Laminar flame speed, Radiation heat loss, Radiation-induced inward flow, refrigerant

* Corresponding author.
E-mail address: jjayachandran@wpi.edu

Novelty and Significance Statement:
This study: 1) expands the current understanding of the effect of radiation heat loss on hydrofluorocarbon (HFC)/air flames and analyzes in detail the contribution from fluorinated species and coupling between radiation heat loss and chemical kinetics; 2) introduces a novel model that can accurately estimate the radiation-induced inward flow for spherically expanding HFC/air flames; and 3) investigates the limits of applicability of the model, or the uncertainty that results when using the model for different mixtures and thermodynamic conditions. The model as well as the knowledge gained can be utilized to accurately measure laminar flame speeds, and hence quantify the flammability of HFCs, which are used as environmentally-friendly refrigerants and flame suppressants. (112 words)

Author Contributions:
JT: Software; Validation; Investigation; Methodology; Data Analysis; Writing
VG: Software; Validation; Writing-Review
JJ: Conceptualization; Software; Investigation; Methodology; Data Analysis; Writing; Resources; Supervision

1. Introduction

In the last decade, several major international treaties such as the Kigali Agreement (an accompaniment to the Montreal Protocol) have promoted the adoption of refrigerants with both lower ozone-depletion potential (ODP) and lower global warming potential (GWP) [1]. A group of hydrofluorocarbon (HFC) compounds have been identified with viable ODP and GWP characteristics [2-6]. However, this particular group of HFCs are *mildly* reactive relative to hydrocarbons and obey the general inverse relationship between reactivity and GWP [2,4,6-10]. As these mildly reactive HFCs pose potential fire risks, the reactivity and flammability limits of these compounds need to be quantified in order to establish proper safety regulations [3,7,8]. The reactivity of HFCs can be generalized according to the fluorine-to-hydrogen (F/H) ratio, where a higher F/H ratio is generally associated with lower HFC reactivity [2,4,7,8], although molecular structure can have a pronounced effect on reactivity (e.g., a relative reduction in reactivity is observed for H-deficient HFCs containing a CF_3 group [11]). Candidate HFC refrigerants have been shown to possess relatively low F/H ratios ($1 \leq F/H \leq 2$) to minimize GWP (i.e., mildly reactive HFCs have shorter atmospheric lifetime) and are often blended with non-flammable compounds to minimize fire risks [2-4]. The flammability characteristics of these candidate HFCs have been assessed through the laminar flame speed (S_u^0), a fundamental combustion property used for kinetic model validation and turbulent combustion scaling [9,10,12]. Accurate measurements of S_u^0s are essential to quantify the reactivity of HFC/air mixtures and develop high-fidelity chemical kinetic models [9].

Spherically expanding flames (SEF) have been widely used to determine S_u^0. This configuration uses small amounts of reactants [10,12,13] and allows for S_u^0 measurements for a wide range of pressures (e.g., [14]). In addition, this configuration effectively contains potentially hazardous burned gas products of HFC/air mixtures, such as hydrogen fluoride (HF), until they can be safely evacuated from the chamber [10,15]. However, S_u^0s derived from experimental measurements of HFC/air flames using the SEF method are often accompanied by large errors and uncertainties. This is due to difficulties in interpreting the experimental measurements of these characteristically slow HFC/air flames while accounting for the effects of radiation heat loss [13,16,17] and buoyancy-induced flow [18,19]. Slowly-propagating spherical flames have previously been shown to deform due to non-uniform gravitational forces [18,20-22]. This, however, can be mitigated by performing experiments under free fall, such as those in a drop tower [18-22]. The constant pressure (CON-P) SEF configuration is particularly attractive for HFC/air flames as the optical access provides a means to ensure that the flames are spherical and free of wrinkles.

Reductions in flame propagation speed due to radiation heat loss have been extensively studied for strongly burning and near-limit hydrocarbon/air flames [23-28]. Flame propagation is affected by radiation heat loss and conduction from the flame zone, referred to as flame zone losses henceforth. This results in a reduction of the maximum flame temperature and the overall reactivity, and consequently the S_u^0 [24,25,28]. For SEFs in particular, cooling of the burned gas due to radiation heat loss induces an inward flow (radiation-induced inward flow) directed towards the center of the flame. If such data isn't interpreted correctly, or corrected for, the radiation-induced inward flow can result in systematically lower values of derived S_u^0s [24,26,27,29]. Large flame zone losses are characteristic of weakly propagating flames, where the time scale of burned gas cooling is comparable to that of flame propagation [23-25,30]. For instance, large flame zone losses (upwards of 15% reduction in S_u^0 [23]) are often observed in flames of hydrocarbon/air with

compositions approaching the lower flammability limit [23-25,28,30]. Furthermore, large flame zone losses were shown to be present for NH_3/air flames, with particularly large reductions in S_u^0 at near stoichiometric conditions compared to hydrocarbon/air flames of the same equivalence ratio [31]. In addition, for weakly propagating flames, the effect of radiation-induced inward flow has been shown to cause large errors in S_u^0s derived using the SEF experiment [24,29,32]. However, few studies exist that investigated the effect of radiation heat loss on slowly-propagating HFC/air flames [13,16,17,32]. Specifically, the radiation heat loss contribution from major fluorinated and burned gas species have yet to be quantified, and percent reductions in S_u^0 and maximum flame temperature (T_{max}) due to radiation heat loss have not been analyzed for a wide range of initial mixture compositions. Therefore, there is a need to analyze the effects of radiation heat loss on HFC/air flames.

While simultaneous measurement of flow velocity and expansion rate can enable accurate determination of S_u^0 [26], such measurements are especially challenging in free-fall experiments. In this case, radiation-induced inward flow can be accounted for while interpreting SEF data using analytical or numerical models which utilize the Optically-Thin Limit (OTL) assumption, which provides an analytical formulation for emission-dominated radiative heat loss flux, $\dot{q}_{rad}$ (e.g., [13,17,32]. Radiation reabsorption is ignored in the OTL model, but this effect may need to be considered in future work for weak HFC/air flames with relatively large optical thickness [33]. Burgess Jr. et al. [33] have considered radiation reabsorption in spherical HFC/air flames, but limited their analysis to solely CO_2 reabsorption, as spectrally-resolved radiation properties are not available for HFC refrigerants. Estimates for flame speed reductions due to the inward flow in radiative flames have been performed in previous studies [16,27,29]. For correcting the inward flow effect in SEFs, Santner et al. [27] derived an analytical model to quantify the radiation-induced inward flow velocity at the flame ($u_b = u_{rad,flame}$) as a function of flame stretch (K) in hydrocarbon/air mixtures for the CON-P SEF configuration; where $u_{rad}(r)$ is the radiation induced flow velocity which varies as a function of the radial coordinate. This model evaluates burned gas parameters, including the Planck mean absorption coefficient (κ_p), at the equilibrium state of the gas mixture. Although Santner et al.'s model also includes an analytical method for estimating flame speed reduction due to flame zone losses, accurate knowledge of kinetic information such as the sensitivity of burning flux to flame temperature is required [27]. Since kinetic models for HFCs are in their early stage of development and have large uncertainties, such estimates can lead to large errors. Santner et al.'s model to estimate inward flow is derived from a simplified energy conservation equation, which assumes that conductive and convective heat transfer effects are negligible in the burned gas compared to radiation heat loss. The computed u_b can then be subtracted from the flame propagation speed (dR_f/dt) derived from flame radius (R_f) vs. time (t) data in order to circumvent the inward flow effect, thus giving the stretched burned flame speed (S_b). The unstretched burned flame speed (S_b^0) can then be derived through extrapolation to $K = 0$ to subtract the effects of flame stretch. Santner et al. [27] showed that using this model to account for the radiation-induced flow effect improved the accuracy of derived S_u^0s for hydrocarbon/air flames at elevated pressures. Hesse et al. [16] applied Santner et al.'s model to estimate u_b and derive S_u^0s of CH_2F_2 (R-32)/air flames at elevated initial unburned gas temperatures (T_u) and pressures (P). However, it is not clear whether the assumptions utilized in Santner et al.'s model are valid for weaker, less reactive flames like non-stoichiometric R-32/air flames at P = 1 bar and T_u = 298 K, or for CH_2CFCF_3 (R-1234yf)/air flames. Models with fewer assumptions might be necessary to properly quantify u_b for HFC/air flames at various conditions of interest.

Numerical simulations utilizing detailed chemical kinetic models have been used to compute the spatial profile for gas velocity ($u(r)$) as a function of time, from which u_b has been derived as the minimum of the gas velocity profile as often done in the literature [17,24,32]. However, reaction rates involving fluorine chemistry are often estimated within detailed chemical kinetic models, potentially introducing large uncertainties and inaccuracies in predictions of flame properties and $u(r)$. Therefore, such models are not suitable for interpreting experimental data. Xiouris et al. [34] developed a Hybrid ThermoDynamic-Radiation (HTDR) model, which interprets experimental data by quantifying the effect of radiative cooling for the constant volume (CON-V) SEF configuration. The HTDR model accounts for finite-rate radiation heat loss using a time scale derived from experimental measurements. The model thus avoids potentially unreliable chemical kinetic data and utilizes fewer assumptions compared to analytical models for the CON-V SEF method, which are reviewed in detail by Faghih and Chen [35]. However, a similar model does not exist for interpreting experimental data using the CON-P SEF method, leaving Santner et al.'s analytical model as the only option to interpret experimental data without utilizing chemical kinetic models.

To properly quantify the reactivity of HFC/air mixtures, S_u^0 must be accurately derived accounting for the effects of radiation. To this end, the major objectives of this study were to: (1) quantify the effects of flame zone losses due to radiation in planar HFC/air flames through reductions in S_u^0 and T_{max} for various initial mixture compositions, and (2) develop and validate a model, one with fewer assumptions than currently available analytical models, that can interpret CON-P SEF experimental data and accurately quantify and correct for radiation-induced inward flow to derive S_u^0.

2. Numerical Approach

2.1. Planar flames

To explore aspects of radiation heat loss in planar HFC/air flames, 1-D, steady, freely propagating flame simulations were performed using the free flame module of Cantera [36]. For various initial compositions of R-32/air and R-1234yf/air mixtures, simulations with and without radiation heat loss were performed, allowing flame zone heat losses to be quantified through the reduction in S_u^0. The equivalence ratio (φ) of R-32/air and R-1234yf/air mixtures was determined based on the stoichiometric major species models of Womeldorf and Grosshandler [37] and Takizawa et al. [2], respectively. The stoichiometric combustion reactions, assuming complete combustion, for R-32 and R-1234yf are expressed by Eqns. (1) and (2), respectively.

$$\mathrm{CH_2F_2 + O_2 \rightarrow 2\ HF + CO_2} \tag{1}$$

$$\mathrm{CH_2CFCF_3 + 2.5\ O_2 \rightarrow 2\ HF + COF_2 + 2\ CO_2} \tag{2}$$

Detailed chemical kinetic models including fluorine chemistry relevant for R-32/air and R-1234yf/air flames developed by Babushok et al. [9,38,39] were utilized. The full detailed R-1234yf chemical model can be found as text in the NIST technical note (i.e., Babushok et al. [39]). The

R-1234yf chemical model was reduced utilizing the Directed Relations Graph (DRG) method, thus minimizing computational costs for R-1234yf/air numerical simulations [40]. Details regarding the reduction of the R-1234yf chemical model using the DRG method, as well as validation of the reduced chemical model, are provided in the Supplementary Material document in subsection G (SM-G). Radiation heat loss was accounted for by utilizing the OTL model. The Cantera source code was modified to include κ_ps for HF, obtained from Fuss & Hamins [41], and COF_2, calculated by Takahashi et al. [42] using data from Modica & Brochu [43]. Adaptive gridding with strict refinement criteria was used to ensure that all solutions were grid-independent. For lean OTL radiation cases, the lower flammability limit was estimated by lowering φ until a converged 1-D solution was no longer possible.

2.2. Spherically expanding flames

Transient, 1-D, SEF simulations (henceforth referred to as Detailed Numerical Simulations or DNS) at constant pressure were performed using the reacting flow code SLTORC, a modified version of the LTORC code [44], which solves the governing spherically symmetric low Mach number conservation equations of mass, species, and energy in Lagrangian coordinates [45]. These equations are described in the Supplementary Material document in subsection A (SM-A). SLTORC utilizes the simpler balanced operator splitting scheme of Wu et al. [46] to overcome gridding and initialization difficulties present in previous versions of the code (e.g., TORC [26], LTORC [44]), which solves governing equations using a fully coupled Differential Algebraic Equation (DAE) solver. CON-P SEFs are initialized by a kernel of hot burned gas, and a hyperbolic tangent profile is utilized to transition smoothly between the burned and unburned gas states. The ignition energy is controlled through parameters specifying the initial kernel radius and temperature, which were chosen so that ignition-related effects would be minimized, enabling quasi-steady propagation to be reached at radii relevant to constant-pressure SEF experiments. A discussion of parameters used to specify ignition energy is provided in SM-C. The time-evolution of R_f is determined using a user-specified isotherm. Convergence tests were conducted to determine proper values for parameters controlling grid refinement and time step size to allow for grid-independent solutions. Solution convergence test results varying spatial and temporal refinement criteria and isotherm temperature are provided in the SM-C. DNS results were then post-processed to determine the evolution of dR_f/dt and u_b with decreasing K. Validation of SLTORC through comparison of results with the well-established freely propagating flame module of Cantera can be found in SM-B.

2.3. Spherical radiation-induced flow model

An open-source Spherical RADiation-Induced Flow (SRADIF) model[1] was developed to quantify $u_{rad}(r)$ in spherically expanding HFC/air flames. u_b can then be derived from $u_{rad}(r)$ thus enabling accurate determination of S_u^0 from CON-P SEF experimental data. The SRADIF model is inspired by the HTDR model for the CON-V SEF method developed by Xiouris et al. [34]. SRADIF uses R_f vs. t data, either from experiments or DNS, as input to estimate $u_{rad}(r)$.

[1] The SRADIF model code can be accessed online and downloaded from: https://github.com/jagan-crl/SRADIF

The model discretizes the total gas volume into N layers of thin spherical shells of equal width. SRADIF combines thermodynamic equilibrium and finite rate OTL radiation heat loss calculations to estimate u_b. Thermal conduction between the shells was excluded from the model, as studies showed that its inclusion caused a negligible change in the results. All thermodynamic calculations are performed using the thermodynamics toolkit of Cantera [36]. The main overarching loop of the SRADIF model is described in steps below and also outlined in Algorithm 1. Each iteration corresponds to the combustion of the i^{th} ($1 \le i \le N$) unburned gas shell. In Algorithm 1, variables with the hat symbol (e.g., $\hat{T}_i$, $\hat{\rho}_i$, $\hat{T}_j$, etc.) specify the intermediate state of gas shells after equilibrium operations (i.e., the combustion of shell i in Step 1 or the dissociation of burned gas shells j in Step 2) but before radiative cooling operations. For the i^{th} iteration of the SRADIF algorithm, the following operations are performed:

1. The combustion of the i^{th} gas shell is modeled as an equilibrium process under the constraints of constant P and enthalpy (h). Once equilibrated, the gas shell achieves its maximum temperature ($\hat{T}_i$), at which burned gas species mole fractions correspond to those at the adiabatic flame temperature (i.e., $\hat{T}_i = T_{ad}$). Due to the constant P and h constraint, the volume of the combusted gas shell ($\hat{V}_{shell,i}$) increases by a factor $\rho_i/\hat{\rho}_i$, where ρ_i and $\hat{\rho}_i$ denote the densities of gas shell i before and after the equilibrium operation, respectively. As a result, the total gas volume also increases by the same amount.
2. All previously burned gas shells j from $1 \le j \le i-1$ are then allowed to equilibrate under constant P and h constraints. This step accounts for the change in equilibrium state due to changes in T due to radiative cooling during the $i-1$ iteration. Thus, the changes in extents of burned gas (i.e., CO_2, HF, COF_2, etc.) dissociation will be captured. The new burned gas shell temperatures ($\hat{T}_j$) and species mole fractions ($\hat{X}_j$) are recorded, and the new burned gas shell volumes ($\hat{V}_{shell,j}$) change by a factor $\rho_j/\hat{\rho}_j$, where ρ_j and $\hat{\rho}_j$ denote the densities of burned gas shells j before and after the equilibrium (dissociation) operation similarly to Step 1. The total burned gas volume including gas shell i ($\hat{V}_{f,i}$), is then calculated, from which the current location of gas shell i before radiative cooling (i.e., the intermediate flame radius $\hat{R}_{f,i}$) is determined.
3. The rate of change of temperature due to radiative cooling in burned gas shell j ($(\partial T/\partial t)_{rad,j}$) is calculated for each burned gas shell according to Eq. (3). The radiative heat loss is calculated using the OTL radiation model, in which individual heat loss contributions are calculated for major products (CO_2, HF, H_2O, CO, and COF_2) using temperature-dependent functions for κ_p for each radiating species k [23,34]. In Eq. (3), $\hat{c}_{p,j}$ is mixture-averaged specific heat at constant pressure of shell j, $\hat{X}_{jk}$ is the mole fraction of radiating species k in shell j, $\hat{\kappa}_{jk}$ is the Planck mean absorption coefficient of radiating species k in shell j, σ is the Stefan-Boltzmann constant, and T_0 is the temperature of the chamber wall.

$$\left(\frac{\partial T}{\partial t}\right)_{rad,j} = \frac{1}{\hat{\rho}_j \hat{c}_{p,j}}\left(4\sigma P \sum\nolimits_k \hat{X}_{jk}\hat{\kappa}_{jk}\left(\hat{T}_j^4 - T_0^4\right)\right) \tag{3}$$

4. The time scale for radiative cooling (Δt_{rad}) is deduced from experimental data for R_f vs. t. This approach is advantageous because it eliminates the dependence on chemical kinetic models, which may have large uncertainties due to inaccuracies associated with reaction rates. Specifically, the radiative cooling time is $\Delta t_{rad} = t_i - t_{i-1}$, where t_{i-1} is the time corresponding to $R_{f,i-1}$ (e.g., the combustion of the i – 1 shell). Subsequently, $R_{f,i}$ is the flame radius at t_i accounting for combustion of the i^{th} shell, as well as radiative cooling and burned gas contraction over Δt_{rad}, during which the flame propagates from $R_{f,i-1}$ to $R_{f,i}$. Since burned gas contraction due to radiative cooling and flame propagation are coupled processes, an iterative approach is required to obtain converged values for the pair (Δt_{rad}, $R_{f,i}$). An initial guess for Δt_{rad} is used as input to the radiative cooling algorithm, in which $(\partial T/\partial t)_{rad,j}$ is applied to all burned gas shells to determine the burned gas volume after radiative cooling ($V_{f,i}$). It is important to note that $V_{f,i}$ and subsequently $R_{f,i}$ are no longer denoted by hats after radiative cooling has been applied. The iterative algorithm then solves for a new estimate for Δt_{rad} by using the R_f vs. t experimental data and ($R_{f,i} - R_{f,i-1}$). Convergence for the pair (Δt_{rad}, $R_{f,i}$) is achieved when the radiative cooling time from the previous cooling step iteration ($\Delta \tilde{t}_{rad}$) differs from Δt_{rad} by less than the specified tolerance (t_{tol}). This iterative process is a key component of SRADIF, allowing the time scale for radiative cooling to be determined using just thermodynamics, OTL radiation heat flux, and the change in R_f measured in experiments.
5. The magnitude of the radiation-induced flow velocity at $R_{f,i}$ ($u_{b,i}$) is calculated by dividing the total burned gas contraction due to radiative cooling (i.e., $\hat{R}_{f,i} - R_{f,i}$) by the converged value of Δt_{rad}. Note that $u_{b,i}$ corresponds to the minimum of $u_{rad}(r)$ (or maximum in the absolute sense) and occurs at the location of the flame, which in this model is infinitely thin.

for $1 < i < N$ *shells* **:**
  Equilibrate unburned shell i // See Step 1
  $\hat{V}_{shell,i} = V_{shell,i}(\frac{\rho_i}{\hat{\rho}_i})$
  for $1 < j < i - 1$ *shells* **:**
    Equilibrate burned shells j // See Step 2
    $\hat{V}_{shell,j} = V_{shell,j}(\frac{\rho_j}{\hat{\rho}_j})$
  end
  $\hat{V}_{f,i} = \sum_{j=1}^{i} \hat{V}_{shell,j}$
  $\hat{R}_{f,i} = (\frac{3}{4\pi}\hat{V}_{f,i})^{1/3}$
  for $1 < j < i$ *shells* **:**
    $(\frac{dT}{dt})_{rad,j} = \frac{1}{\hat{\rho}_j \hat{c}_{p,j}}(4\sigma P \sum_k \hat{X}_{jk}\hat{\kappa}_{jk}(\hat{T}_j^4 - T_0^4))$ // See Step 3
  end
  while $\Delta t_{rad} - \Delta\tilde{t}_{rad} > t_{tol}$: // See Step 4
  do
    $\Delta\tilde{t}_{rad} = \Delta t_{rad}$
    for $1 < j < i$ *shells* **:**
      $T_j = \hat{T}_j - (\frac{dT}{dt})_{rad,j}\Delta t_{rad}$
      $V_{shell,j} = \hat{V}_{shell,j}(\frac{\hat{T}_j}{T_j})$
    end
    $V_{f,i} = \sum_{j=1}^{i} V_{shell,j}$
    $R_{f,i} = (\frac{3}{4\pi}V_{f,i})^{1/3}$
    Estimate Δt_{rad} using interpolation
  end
  $u_{b,i} = (\hat{R}_{f,i} - R_{f,i})/\Delta t_{rad}$ // See Step 5
end

Algorithm 1: SRADIF numerical model. See the numbered list for further details corresponding to Steps 1-5.

The algorithm is repeated for each subsequent shell until either all N shells have been burned or simulated burned gas radius exceeds the final radius of the input R_f vs t data. To validate the model, CON-P SEF DNS results for R_f vs t were used as the "experimental" data. This allowed for the u_b computed from the SRADIF model to be directly compared to that derived from DNS results.

2.4. Radiation-induced flow velocity derivation from DNS results

The SRADIF model was validated by testing its ability to estimate u_b when provided with "data" obtained from DNS. Thus, the estimated u_b could be compared against the "true" value obtained from DNS results. In SEFs, the gas velocity is a function of r and t (i.e., $u = u(r, t)$). At

a particular t, the gas velocity $u(r)$, which quantifies the total induced flow driven by changes in ρ, can be computed using Eq. (4), derived from the continuity equation for CON-P SEFs [45]:

$$u(r) = -\frac{1}{\rho r^2}\int_0^r \frac{\partial(\rho \bar{r}^2)}{\partial t}\bar{r}^2 d\bar{r} \tag{4}$$

The gas velocity $u(r)$ may also be viewed as the flow induced by the contribution of all heat flux and heat source/sink terms of the energy conservation equation (details regarding the complete governing conservation of energy equation, as well as a formula for $u(r)$ derived from all heat terms, is given in SM-F). The value of u_b is commonly derived as the minimum of $u(r)$, which occurs in the burned gas in the proximity of the flame zone [17,24,32]. However, there is an issue with the conventional method of estimating u_b as the minimum of $u(r)$. The location of this minimum is determined by the competition between radiation-induced inward flow and heat release-induced outward flow. Thus, the total gas velocity $u(r)$ may not be the relevant flow velocity for deriving u_b, which should only contain information about flow generated due to radiation heat loss. By isolating the radiation heat loss term in the governing energy equation, the radiation losses in the burned gas can be quantified by the radiation-induced gas flow profile $u_{rad}(r)$. For CON-P SEFs, this corresponds to flow driven by changes in ρ due to radiative cooling in the burned gas. To validate the SRADIF model, a formula for $u_{rad}(r)$ must be derived. Santner et al. [27] and Yu et al. [29] both derived equations for u_b from a simplified energy conservation equation, in which the terms for convection, conduction, mass diffusion, and chemical heat release were deemed to be negligible compared to the radiation heat loss term ($\dot{q}_{rad}$). Eqns. (5) and (6) denote the continuity and energy conservation equations, respectively [24]. The energy conservation equation takes into account changes in temperature solely due to radiation heat loss.

$$\frac{\partial \rho}{\partial t} + \frac{1}{r^2}\frac{\partial(\rho u r^2)}{\partial r} = 0 \tag{5}$$

$$\rho c_p \frac{\partial T}{\partial t} = -\dot{q}_{rad} \tag{6}$$

Substituting Eq. (6) into Eq. (5) via the ideal gas law, Eq. (7) for $u_{rad}(r)$ was derived.

$$u_{rad,no-conv}(r) = -\frac{1}{\rho r^2}\int_0^r \frac{\dot{q}_{rad}}{c_p T}\bar{r}^2 d\bar{r} \tag{7}$$

However, this approach ignores a potentially important coupling between the convective terms of the continuity and energy conservation equations. Eq. (8) shows the conservation of energy equation including the radiation heat loss and convective terms.

$$\rho c_p \frac{\partial T}{\partial t} + \rho u c_p \frac{\partial T}{\partial r} = -q_{rad} \tag{8}$$

A new equation (Eq. (9)) for $u_{rad}(r)$, now including convective term coupling, is thus derived.

$$u_{rad,conv}(r) = -\frac{1}{r^2}\int_0^r \frac{\dot{q}_{rad}}{\rho c_p T}\bar{r}^2 d\bar{r} \quad (9)$$

Detailed derivations for Eqns. (7) and (9) are provided in SM-F.

3. Results and discussion

3.1. Planar HFC/air flames

To quantify the radiative heat loss from the flame zone in HFC/air flames, S_u^0 and T_{max} were computed for 1-D planar R-32/air and R-1234/air flames for various φ using both the adiabatic and OTL radiation assumptions. T_u = 400 K was used for all R-1234yf/air mixtures, as 1-D flame solutions could not be obtained (even for φ =1) with the chosen chemical model for T_u = 300 K, utilizing the OTL radiation model. These R-1234yf flames (T_u = 300 K), simulated using both the full and reduced chemical kinetic models and OTL radiation model, appear to be not flammable as a result. The fact that such flames have been experimentally established calls into question the validity of the models, especially the chemical kinetic model. The fact that such flames have been experimentally established calls into question the validity of the models, including the chemical kinetic model and the OTL radiation model. As the OTL model does not consider radiation re-absorption, the model inherently overestimates the actual radiation heat loss present in experiments. A more detailed discussion of the "non-flammable" result is given in SM-G. S_u^0 and T_{max} values as a function of φ for P = 1 atm are shown in Figs. 1-2a and Figs. 1-2b for R-32/air and R-1234/air flames, respectively. In addition, percent reductions in S_u^0 are indicated to highlight the regions of smallest and largest radiative heat loss effects. S_u^0 reductions are shown to be substantial, with percent reductions as large as 40% for the φ range of interest. The reduction in S_u^0 is greatest near the estimated lower flammability limit, which occurred between φ values of 0.7 and 0.8 in both R-32/air and R-1234/air flame cases. These lower limits were approximated as the minimum φ for which a grid-independent solution was no longer achievable. Further reductions in φ below these limits gave no steady solution as a flame could not be stabilized, indicating that the mixture was no longer flammable. For comparison, percent reductions in lean methane/air flames are no greater than 3% for the same range of φ [23]. Therefore, the effect of radiative heat loss on S_u^0 is much greater for HFC/air flames compared to typical hydrocarbon/air flames for the same φ. Furthermore, reductions in T_{max} are significant over the entire range of φ for both R-32/air and R-1234/air flames, with reductions as large as 12% and 21%, respectively. Large reductions are observed for R-32/air even near stoichiometric conditions due to its relatively high T_{ad}, which is comparable to that of methane/air flames [23]. Notably, the reduction in T_{max} for lean and stoichiometric R-1234/air flames is much larger compared to rich conditions. In addition, the peak T_{max} for radiative R-1234/air flames occurs at a much larger φ compared to the peak T_{max} for adiabatic flames, which occurs at slightly rich conditions similarly to that of adiabatic and radiative R-32/air flames. This result can be attributed to the slow chemical kinetics associated with CO oxidation, which will be discussed in Sec. 3.2.3.

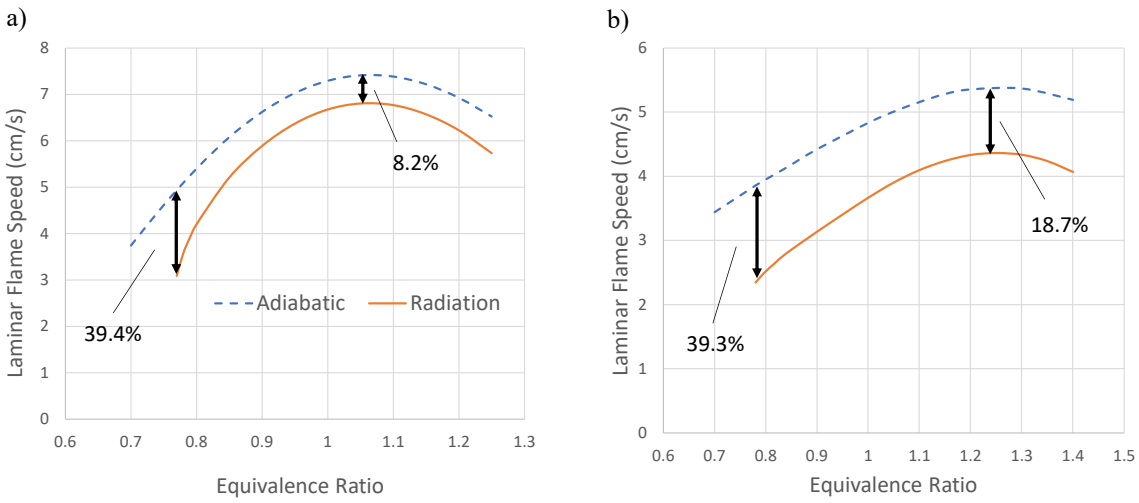

Fig. 1. S_u^0 vs. φ for simulated planar, steady HFC/air flames for adiabatic and radiation heat loss cases: a) R-32/air flame with P = 1 atm and T_u = 300 K, b) R-1234yf/air flame with P = 1 atm and T_u = 400 K.

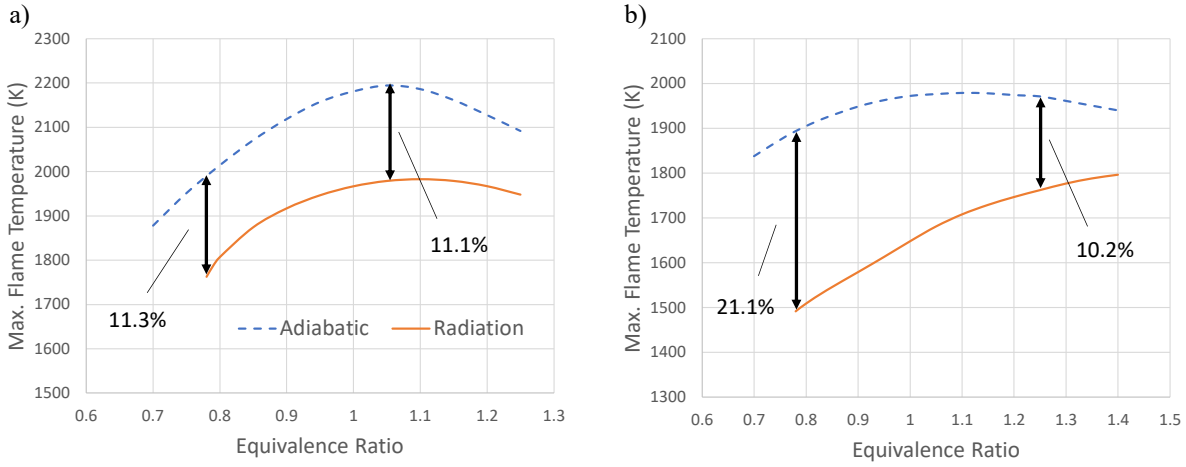

Fig. 2. T_{max} vs. φ for simulated planar, steady HFC/air flames for adiabatic and radiation heat loss cases: a) R-32/air flame with P = 1 atm and T_u = 300 K, b) 1234yf/air flame with P = 1 atm and T_u = 400 K.

The contribution of each radiating species to the total radiation heat loss flux can be determined from the OTL model and are functions of κ_p and X_k for each radiating species k. The major species X_k and species contribution to radiation heat loss ($\dot{q}_{rad,k}$) for planar R-32/air and R-1234yf/air flames are shown in Fig. 3a and Fig. 3b, respectively. The major burned gas products for stoichiometric R-32/air flames are HF and CO_2, while the major burned gas products for stoichiometric R-1234/air flames are HF, CO_2, CO, and COF_2. In both flames, HF is found in larger concentrations in the burned gas than CO_2. However, CO_2 has the largest $\dot{q}_{rad,k}$ and is thus

the greatest contributor to the total radiation heat loss. This is due to the large κ_p of CO_2 at high temperatures compared to other major radiating species, as shown in Fig. 4. In addition, the heat loss contribution of COF_2 is significant in the burned gas of the R-1234yf/air flame, with a $\dot{q}_{rad,k}$ magnitude that is comparable to that of HF. Although, CO is a major product in the R-1234yf/air flame, it makes a relatively small heat loss contribution due to its smaller κ_p. These results emphasize the necessity for accurate values of κ_p for the mentioned fluorinated species as they are shown to significantly contribute to radiation heat loss.

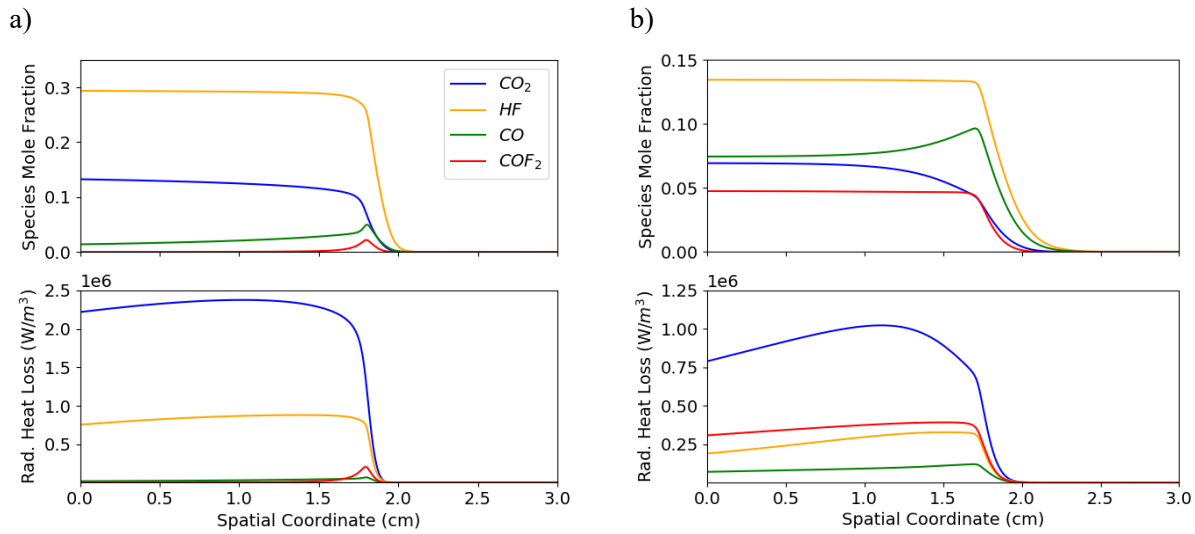

Fig. 3. Major species X_k and $\dot{q}_{rad,k}$ as a function of spatial coordinate for simulated planar, steady, radiating HFC/air flames. a) R-32/air flame with φ =1.0, P = 1 atm, and T_u = 300 K, and b) R-1234yf/air flame with φ =1.0, P = 1 atm, and T_u = 400 K. The flames are stabilized at a spatial coordinate of approx. 1.8 cm with the unburned gas flowing into the domain from the right side. *Refer to online version for plots with color.

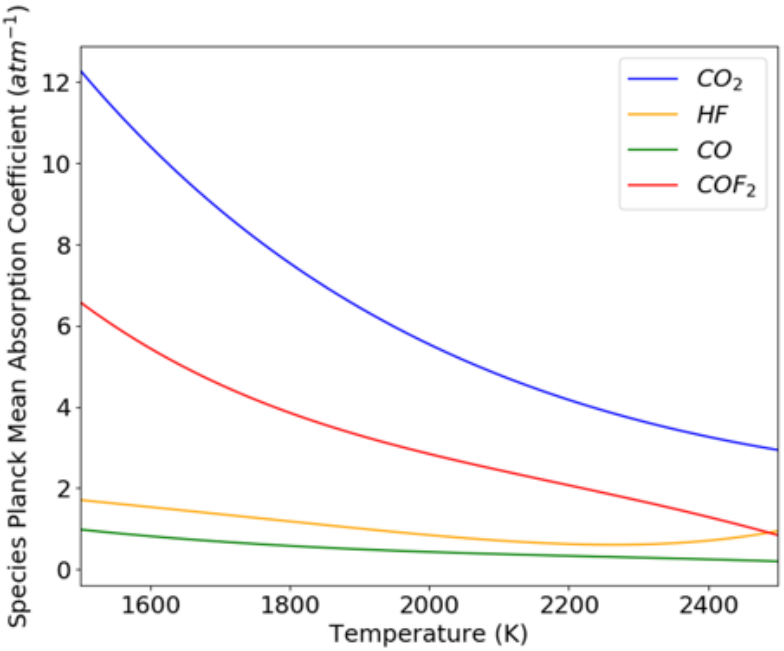

Fig. 4. κ_p vs. T for major radiating species of R-32/air and R-1234yf/air flames. *Refer to online version for plots with color.

3.2. Spherically expanding HFC/air flames

3.2.1. Extracting $u_{rad}(r)$ from DNS results

DNS results were obtained for rich (φ = 1.2) SEFs of R-32/air mixtures and stoichiometric R-1234yf/air mixtures at ambient pressure (P = 1 atm) and high pressure (P = 5 atm) conditions, while accounting for radiation heat loss in the burned gas. The total $\dot{q}_{rad}(r)$ was computed at each time step by summing the heat loss contributions from major radiating species. The variation of $\dot{q}_{rad}(r)$ in the burned gas was examined at specified time instances in which the flame had reached quasi-steady propagation (i.e., ignition-related effects are negligible). As flow velocities are more practical for quantifying the effect of radiation heat loss on dR_f/dt, $u_{rad}(r)$ was derived from $\dot{q}_{rad}(r)$ through the two formulations (Eqns. (7) and (9)). Sample results for $\dot{q}_{rad}(r)$ and $u_{rad}(r)$ for an R-32/air flame with φ =1.2, P = 1 atm, and T_u = 300 K are shown in Fig. 5, in which the derived $u_{rad}(r)$ profiles are compared to that of $u(r)$ (i.e., the total gas velocity induced by density changes from all heat terms in the conservation of energy equation). The greatest difference occurs in the unburned gas (r > 5 cm when flame has reached R_f = 5 cm). Here, $u_{rad,conv}(r)$ (including the convective term) shares the same $1/r^2$ trend as $u(r)$. This trend is to be expected for CON-P SEFs, for which the thermodynamic state of the unburned gas remains constant and spatially uniform. Thus, inward flow should be generated in the unburned gas due to burned gas cooling and shrinkage. Furthermore, the convective term of the energy equation cannot be deemed negligible in such derivations, as convective term coupling between the continuity and energy equations is significant in terms of producing expected flow behavior in the unburned gas. Thus, $u_{rad,conv}(r)$ was chosen as the correct formulation for deriving u_b in CON-P SEFs. Additionally,

in Fig. 5b, there is an appreciable difference between the minima of $u_{rad,conv}(r)$ and $u(r)$. Using the minimum of $u(r)$, which is affected by other heat terms in addition to radiation heat loss (see SM-F for formula for $u(r)$ derived from heat terms), as the conventional method for computing u_b can potentially underpredict u_b by upwards of 30% compared to using the minimum of $u_{rad,conv}(r)$ as seen in Fig. 5b. Therefore, the minimum of $u(r)$ is inadequate for accurately estimating u_b in spherical HFC/air flames. Henceforth, $u_{rad,conv}(r)$ will be referred to as $u_{rad}(r)$, from which u_b is derived.

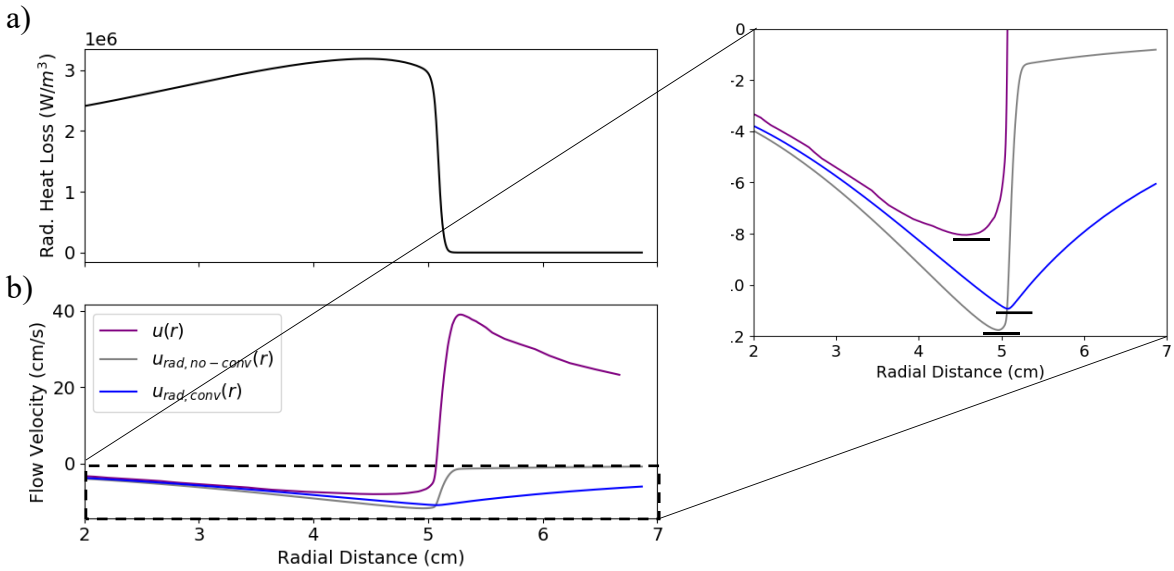

Fig. 5. Spherical, quasi-steady, R-32/air flame with φ =1.2, P = 1 atm, and T_u = 300 K: a) $\dot{q}_{rad}$ vs. r, b) $u(r)$ and $u_{rad}(r)$ vs. r. The flow velocities $u_{rad,no-conv}(r)$ and $u_{rad,conv}(r)$ were computed using Eqns. (7) and (9), respectively, while $u(r)$ is the total gas flow velocity computed according to Eq. (4). *Refer to online version for plots with color.

3.2.2. Validation of the SRADIF model

As mentioned in Sec. 2.4, the SRADIF model needs to be validated using DNS results before it can be used to interpret experimental measurements. Using DNS-generated R_f vs. t as an input, the SRADIF model was used to compute $u_{rad}(r)$ for times at which the flame reached quasi-steady propagation. In addition, DNS results were post-processed directly to compute $u_{rad}(r)$ using Eq. (9). Fig. 6a-d and Fig. 7a-d show a comparison of DNS vs. SRADIF model results for rich, spherical R-32/air flames with P = 1 atm and P = 5 atm, respectively. In Fig. 6a-c, for P = 1 atm, the model accurately predicts T_{max} and major species X_k near the flame zone, with small overpredictions compared to those from DNS. The greatest difference occurs in the heat loss contribution of CO_2 in Fig. 6b, where the maximum value at the flame zone is overpredicted by approx. 12%. However, this does not have a large impact on the minimum $u_{rad}(r)$ (i.e., the magnitude of u_b), which differs from the DNS value by less than 2%, as shown in Fig. 6d. As for the P = 5 atm case, the DNS flame is notably stronger due to an increase in overall reactivity, with major species X_k and T quickly approaching their equilibrium values within

the flame zone. As the SRADIF model evaluates these properties assuming the equilibrium state is achieved at the flame location, the model was able to accurately predict profiles for $X_k(r)$, $\dot{q}_{rad,k}(r)$, $T(r)$, and $u_{rad}(r)$ compared to DNS results for this case as shown in Fig. 7a-d.

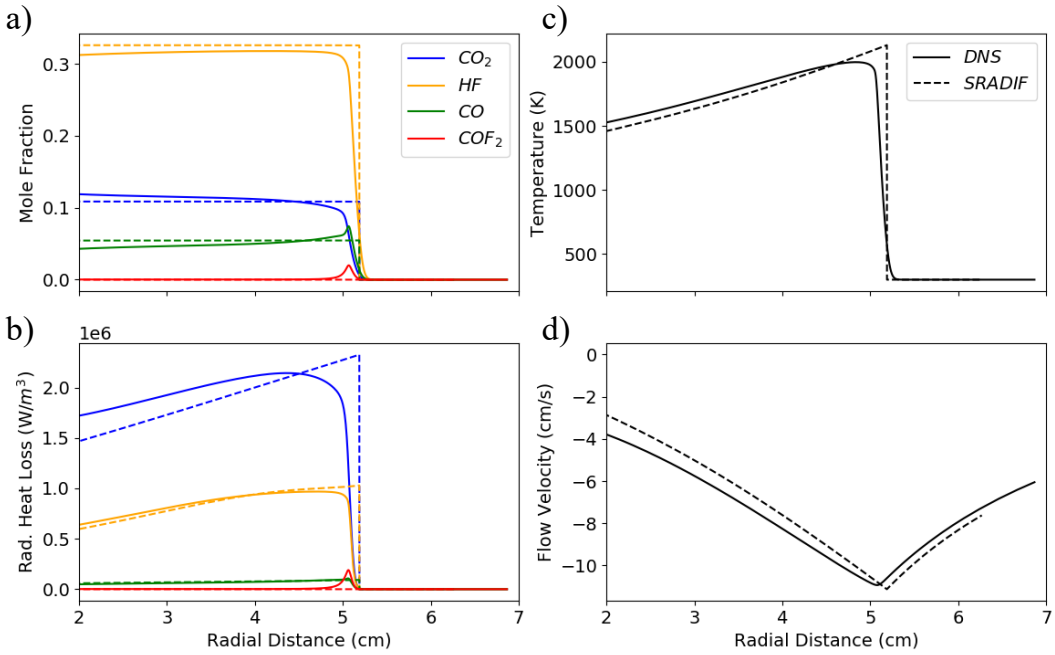

Fig. 6. Spherically expanding (R_f = 5 cm), R-32/air flame with φ =1.2, P = 1 atm, and T_u = 300 K: a) Major radiating species X_k vs. r, b) Major radiating species $\dot{q}_{rad,k}$ vs. r, c) T vs. r, d) u_{rad} vs. r. *Refer to online version for plots with color.

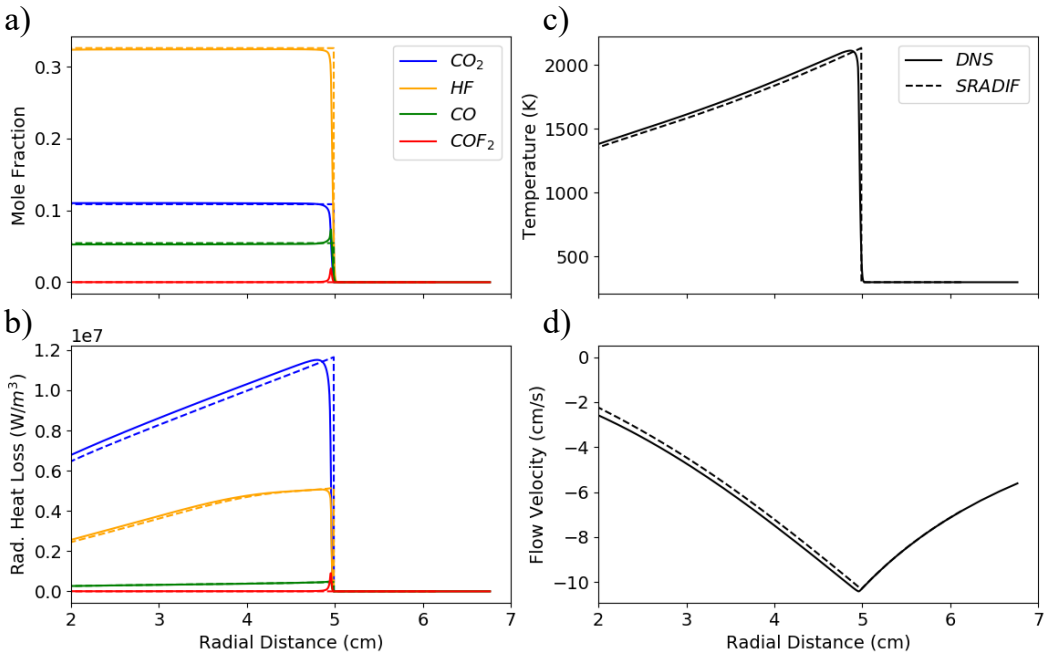

Fig. 7. Spherically expanding (R_f = 5 cm), R-32/air flame with φ =1.2, P = 5 atm, and T_u = 300 K: a) Major radiating species X_k vs. r, b) Major radiating species $\dot{q}_{rad,k}$ vs. r, c) T vs. r, d) u_{rad} vs. r. *Refer to online version for plots with color.

The accuracy of the SRADIF model appears to be correlated to finite chemical kinetic effects. The model assumes that burning a shell is equivalent to the shell attaining the equilibrium state, characterized by T_{ad} and equilibrium X_k. As evident from Fig. 6a-c, this is not the case for the P = 1 atm case. For weaker flames with lower overall reactivity, as well as larger radiation heat loss, a reduction in flame temperature can greatly affect rates of chemical reactions, and consequently, the time required for species to reach their equilibrium values can be significantly increased. Since finite chemical kinetics are only considered in DNS, the SRADIF model will inherently overestimate the maximum radiation heat loss and the magnitude of u_b compared to DNS results. In any case, the SRADIF model is shown to still accurately predict u_b within approx. 5% for moderately weak flames, such as R-32/air flames with P = 1 atm and T_u = 300 K. For these conditions, the accuracy of the u_b estimate was similar across a large range of equivalence ratios ($0.8 \leq \varphi \leq 1.4$), where a maximum difference of approx. 5% was observed at φ = 0.8 (near the estimated lean flammability limit), corresponding to an approx. difference of 0.7% in the derived value for S_b^0. As the CON-P SEF experimental uncertainty is generally much larger [34], small errors in u_b computed from SRADIF are likely to have a minor effect when deriving S_u^0. However, finite chemical kinetic effects may need to be considered for the weakest of HFC/air flames when using the SRADIF model to estimate u_b. This is discussed in more detail in Sec. 3.2.3.

Once u_b is derived, it can then be subtracted from dR_f/dt to give S_b. Note that dR_f/dt is affected by radiation-induced flow and S_b is not. In Fig. 8a-b and Fig. 9a-b, dR_f/dt, S_b, and u_b are plotted vs. K for rich, spherically expanding R-32/air flames at P = 1 atm and P = 5 atm, respectively. The magnitude of u_b in Figs. 8-9b was computed using the SRADIF model and the model of Santner et al. [27], which were compared to the "true" u_b values derived from DNS

results. These values of u_b, shown in Figs. 8-9b, were then subtracted from DNS-extracted dR_f/dt to give different estimates for S_b. These "radiation-corrected" S_b were also compared to S_b assuming adiabatic conditions, as shown in Figs. 8-9a. According to Figs. 8-9b, the SRADIF model provides a vastly improved estimate for the magnitude of u_b in all cases compared to Santner et al.'s model, with very good agreement with DNS results. Santner et al.'s model underpredicts u_b across all cases and was found to differ by upwards of 70% compared to the "true" u_b. This trend was also observed by Hesse et al. [16], who showed that u_b was underpredicted by approx. 40% for an R-32/air flame with φ = 1.0, P = 3 bar, and T_u = 333 K. However, the minimum of u_{total} was used to derive the "true" u_b from DNS results in their analysis [16], which is not correct as pointed out in Sec. 3.2.1. In addition, Figs. 8-9b show how the SRADIF model better predicts the magnitude of u_b for high-pressure R-32/air flames compared to R-32/air flames at 1 atm. This indicates that the SRADIF model provides a better estimate for u_b in stronger, more reactive flames. Furthermore, for quasi-steadily propagating SEFs, S_b derived using the SRADIF model has a slope approximately equal to that of the adiabatic DNS case, according to Figs. 8-9a. This trend was to be expected, as the difference between the radiation-corrected S_b and adiabatic S_b is due to flame zone losses, which are not strongly affected by flame stretch. An extrapolation to $K = 0$ for the SRADIF-corrected, Santner-corrected, and adiabatic S_b curves for the φ = 1.2, P = 1 atm, and T_u = 300 K case is depicted in SM-D. The resulting S_b^0 from extrapolation can then be multiplied by the density ratio (ρ_b/ρ_u) to obtain derived values for S_u^0. Here, ρ_u is the density of the unburned gas mixture and ρ_b is the density of the burned gas mixture, where ρ_b is approximated as the density of the equilibrated mixture (ρ_{ad}) at T_{ad}. S_u^0s extracted this way from SEF DNS results agrees very well with S_u^0 obtained from planar freely propagating flame calculations (see SM-D). Thus, although ρ_b is ill-defined for radiating flames, the density correction using $\rho_b = \rho_{ad}$ is a practical approach to determine S_u^0. Additionally, the SRADIF model was used to interpret raw experimental data obtained from Hegetschweiler & coworkers [32] for an R-32/air SEF with φ = 1.2, P = 1 atm, and T_u = 300 K. The SRADIF-corrected S_b obtained from interpreting experimental data is shown to agree very well with DNS results for this case, which are given in SM-E. Note that the procedure to subtract flame zone losses and obtain the "adiabatic" S_u^0, proposed by Santner et al. [27], and utilized by Hesse et al. [16], is not adopted. Since experimental measurements are affected by flame zone heat loss, it is better to compare inward-flow-corrected experimental measurements (non-adiabatic S_u^0s) to numerical simulations including radiation heat loss, avoiding the potentially erroneous process of subtracting flame zone losses, which requires accurate knowledge of kinetic information, particularly the sensitivity of S_u^0 to T_{ad}.

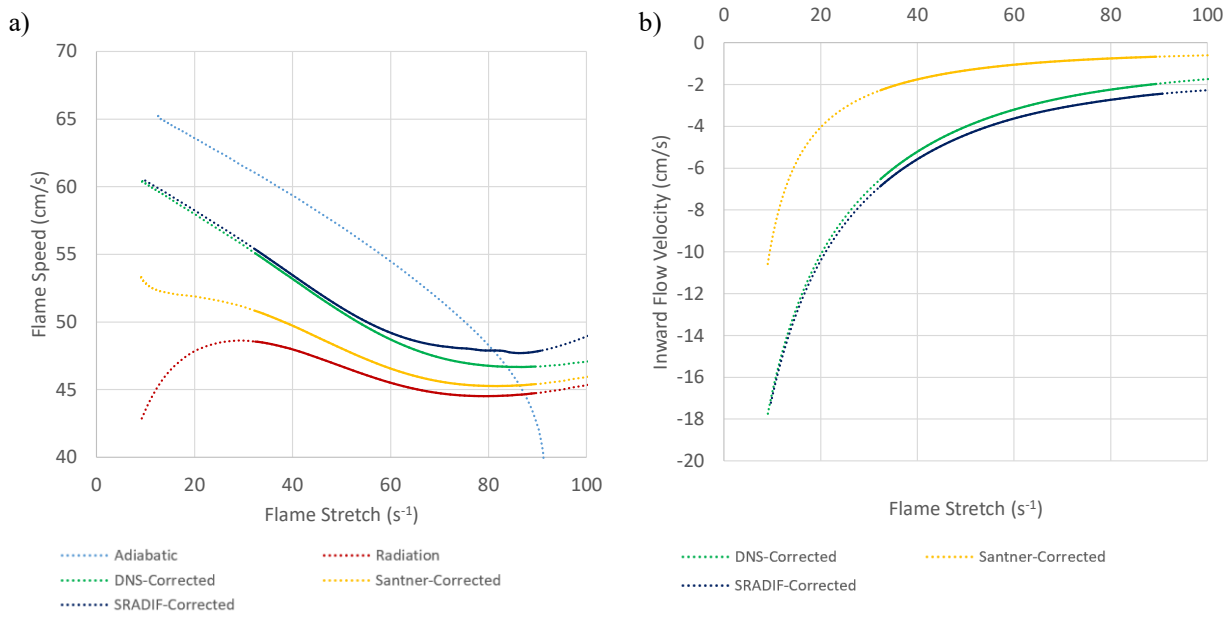

Fig. 8. Spherical, R-32/air flame with φ =1.2, P = 1 atm, and T_u = 300 K: a) dR_f/dt and radiation-corrected S_b vs. K, b) u_b vs. K. "Adiabatic" refers to the S_b curve derived from DNS with radiation heat loss neglected. "Radiation" refers to the dR_f/dt curve derived from DNS with radiation heat loss included. "DNS-Corrected" refers to S_b and u_b curves, in which u_b was derived from DNS results using Eq. (9). "Santner-Corrected" refers to S_b and u_b curves, in which u_b was derived from the analytical model of Santner et al. [27]. "SRADIF-corrected" refers to S_b and u_b curves, in which u_b was derived from the developed SEF radiation model. Solid regions of curves indicate a range of flame radii applicable to typical CON-P SEF experimental setups (1.0 cm < R_f < 3.0 cm). *Refer to online version for plots with color.

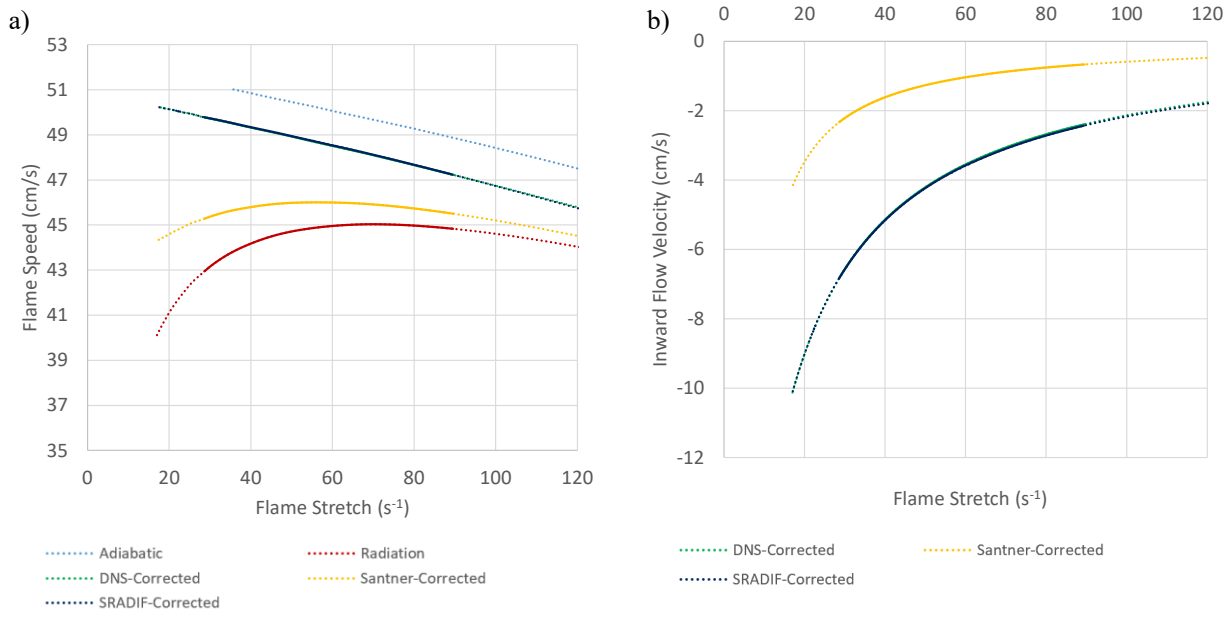

Fig. 9. Spherical, R-32/air flame with φ =1.2, P = 5 atm, and T_u = 300 K: a) dR_f/dt and radiation-corrected S_b vs. K, b) u_b vs. K. "Adiabatic" refers to the S_b curve derived from DNS with radiation heat loss neglected. "Radiation" refers to the dR_f/dt curve derived from DNS with radiation heat loss included. "DNS-Corrected" refers to S_b and u_b curves, in which u_b was derived from DNS results using Eq. (9). "Santner-Corrected" refers to S_b and u_b curves, in which u_b was derived from the analytical model of Santner et al. [27]. "SRADIF-corrected" refers to S_b and u_b curves, in which u_b was derived from the developed SEF radiation model. Solid regions of curves indicate a range of flame radii applicable to typical CON-P SEF experimental setups (1.0 cm < R_f < 3.0 cm). *Refer to online version for plots with color.

3.2.3. Applicability of SRADIF

To evaluate the limits of applicability of SRADIF, the model was used to interpret DNS results for R-1234yf/air flames. These are much weaker flames relative to R-32/air flames, with S_u^0 values of approx. 2-4 cm/s at elevated unburned gas temperatures (T_u = 400 K), as depicted in Fig. 1b. Figures 10a-d and 11a-d show a comparison of DNS vs. SRADIF model results for stoichiometric R-1234yf/air SEFs at P = 1 atm and P = 5 atm conditions, respectively. According to Figs. 10-11a, selected burned gas X_k from DNS are shown to greatly differ from those predicted by SRADIF. The discrepancy between the model and DNS results can be primarily explained by closely inspecting the CO oxidation kinetics. Needham and Westmoreland [47] studied the flame structure and kinetics of planar, stoichiometric R-1234/air flames assuming adiabatic conditions. Their flame calculations highlighted a rather slow conversion of the CO formed in the first zone of the flame to CO_2 in the second zone. The end of the first zone was characterized by the total consumption of R-1234yf, at which a majority of species reached their equilibrium values [47]. CO and CO_2 mole fractions were shown to slowly approach their equilibrium value at a distance more than 10 times greater than the thickness of the first flame zone. This slowness was attributed to the substantially low concentration of H, OH, and O radicals once the source for H, R-1234yf, is consumed. This behavior is characteristic of combustible mixtures with F/H > 1. However, they did not analyze radiative R-1234/air flames, for which a large reduction in T_{max} occurs, as shown in Fig. 2b and Fig. 12a. This could affect CO oxidation kinetics as hypothesized by Needham and Westmoreland [47]. As seen in Fig. 12a, T decreases significantly downstream of the flame. This decrease in T significantly slows down the rate of CO to CO_2 conversion in the second zone, essentially freezing the mixture composition downstream. Thus, the X_{CO2} downstream of the flame is significantly lower than X_{CO2} at chemical equilibrium as shown in Fig. 12b. In other words, a majority of chemical heat released from CO oxidation is suppressed resulting in large reductions in T_{max} for lean and stoichiometric R-1234/air flames as shown in Fig. 2b. This is the reason for large differences in T (up to 20%) between adiabatic and radiating R-1234yf/air flames, as shown in Fig. 2b. This also explains the inability of SRADIF model to estimate radiation-induced flow velocities for R-1234yf/air SEFs. Utilizing equilibrium considerations, SRADIF overestimates both T and X_{CO2} in the burned gas. This leads to an overestimate of the total radiative heat flux, and consequently, an overestimate of u_b. SRADIF also underestimates X_{COF2} downstream of the flame, where a large concentration of COF_2 is predicted from DNS in Fig. 10a due to the slow removal of COF_2 in H-deficient HFCs [48]. However, the differences in X_{COF2} between SRADIF and DNS are shown to cause a minimal difference in COF_2's contribution to radiation heat loss,

as shown in Figs. 10b, especially compared to the large differences from that of CO_2. Even at P = 5 atm, which corresponds to a stronger R-1234yf/air flame relative to 1 atm, the burned gas state differs from that at equilibrium; see Fig. 11. Although the estimates for u_b from SRADIF better match the DNS results at P = 5 atm relative to P = 1 atm, finite rate kinetic effects, specifically from slow CO oxidation kinetics, must be included in the SRADIF model to accurately estimate u_b for R-1234yf/air flames. The same could be the case for other HFC/air mixtures with F/H > 1. This will the subject of future work.

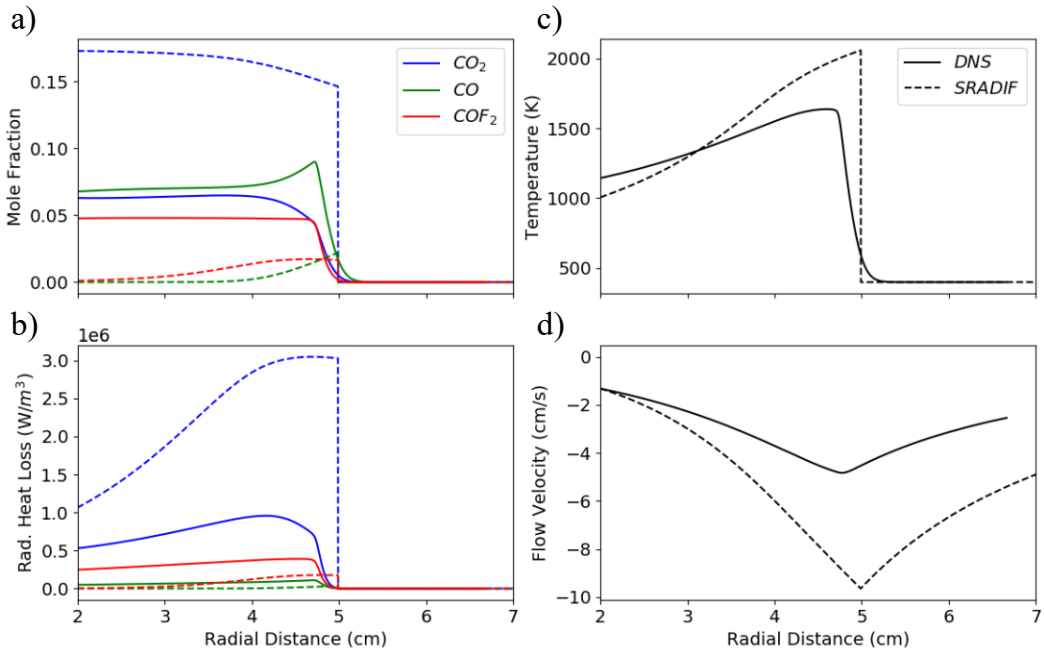

Fig. 10. Spherical, quasi-steady (R_f = 5 cm), R-1234yf/air flame with φ =1.0, P = 1 atm, and T_u = 400 K: a) Major radiating species X_k vs. r, b) Major radiating species $\dot{q}_{rad,k}$ vs. r, c) T vs. r, d) u_{rad} vs. r. *Refer to online version for plots with color.

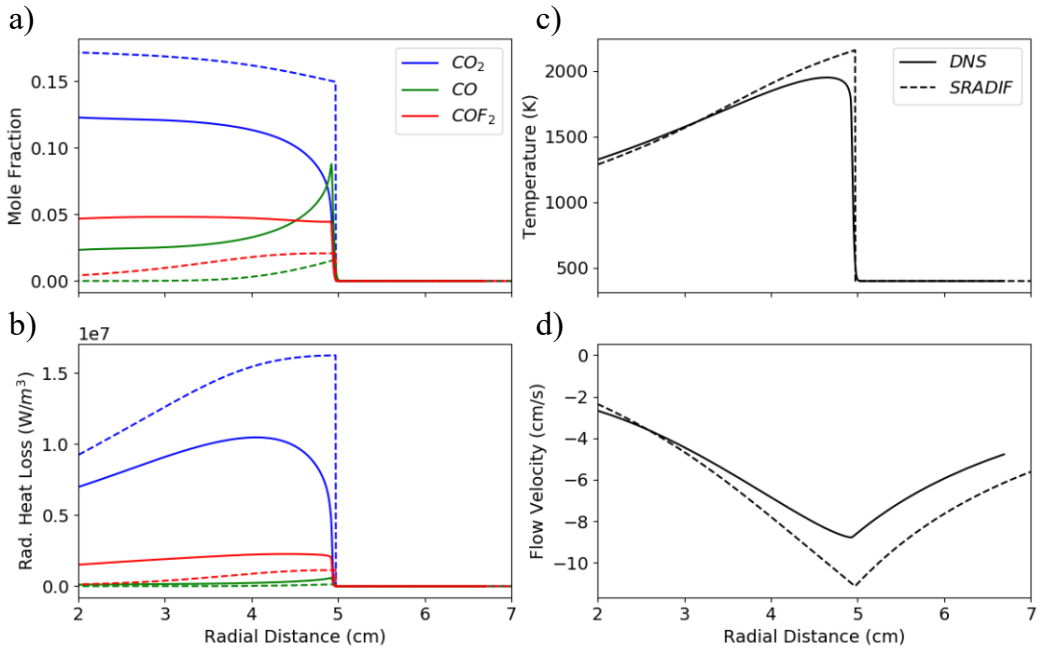

Fig. 11. Spherical, quasi-steady (R_f = 5 cm), R-1234yf/air flame with φ =1.0, P = 5 atm, and T_u = 400 K: a) Major radiating species X_k vs. r, b) Major radiating species $\dot{q}_{rad,k}$ vs. r, c) T vs. r, d) u_{rad} vs. r. *Refer to online version for plots with color.

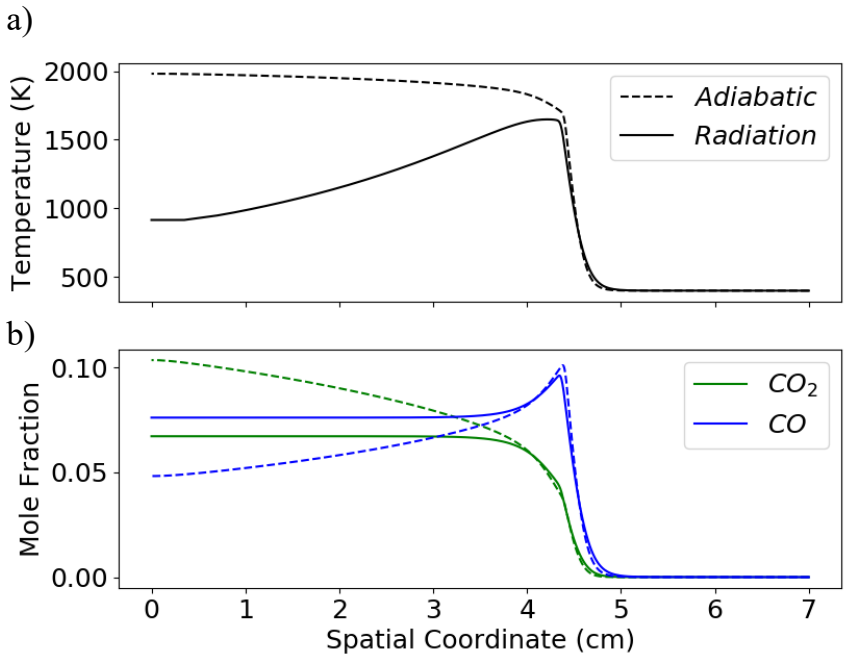

Fig. 12. Steady, planar, R-1234yf/air flame with φ =1.0, P = 1 atm, and T_u = 400 K for adiabatic and radiation heat loss cases: a) T vs. spatial coordinate, b). X_k of CO_2 and CO vs. spatial coordinate. *Refer to online version for plots with color.

4. Conclusions

Computational studies were performed to investigate the effect of radiation heat loss on planar and spherically expanding hydrofluorocarbon/air (HFC/air) flames, which have characteristically low propagation speeds. The mildly flammable HFCs R-32 and R-1234yf were chosen as candidate refrigerants for the study due to their differing fluorine-to-hydrogen (F/H) ratio and key differences in molecular structure. Planar flame simulations, which accounted for radiation heat loss contributions from major radiating species with the optically-thin limit assumption, revealed significant reductions in the laminar flame speed compared to hydrocarbon/air mixtures under similar conditions. Reductions between 8-20% at near stoichiometric conditions and up to 40% at near-limit conditions were observed. It was shown that radiation from fluorinated species such as HF and COF_2 formed a significant fraction of the total radiation heat flux. Thus, radiation heat loss from these species need to be modeled to accurately estimate the total radiation heat flux from HFC/air flames.

For spherically expanding HFC/air flames, radiation heat loss from the burned gas is shown to result in significant inward flow velocities which can introduce systematic errors when interpreting flame propagation speed measurements to derive the laminar flame speeds. So, a spherical radiation-induced flow model (SRADIF) was developed to estimate the burned gas inward flow velocities. This model discretizes the spherical domain into shells and utilizes thermodynamic and optically thin limit radiation heat loss calculations to estimate the heat loss and induced flow. Experimental flame radius versus time data is used to estimate the time scale of cooling, which is required to calculate heat loss, circumventing the need to use chemical kinetic models that can have large uncertainties. The model is shown to accurately predict the inward flow velocity for R-32/air mixtures over a range of conditions and performs significantly better compared to existing analytical models.

SRADIF was, however, unable to accurately estimate the induced flow velocities for R-1234yf/air mixtures, which are relatively slowly propagating with laminar flame speeds of 2-4 cm/s. Utilizing results of flame simulations, it was shown that for these flames the radiation heat loss resulted in burned gas compositions different from that at equilibrium. Analysis revealed incomplete CO to CO_2 in the burned gas behind the flame. For the R-1234yf/air flame ($F/H > 1$), the CO to CO_2 conversion occurs over many flame thicknesses. So, the radiation heat loss induced temperature drop slows reaction rates governing CO to CO_2 conversion, freezing the products at a metastable state before they attain equilibrium. Since SRADIF utilizes thermodynamic equilibration to estimate the burned gas state, caution must be taken while using the model to interpret experimental data for R-1234yf/air flames and potentially other HFC/air flames with $F/H > 1$.

5. Acknowledgments

This work was supported by the National Science Foundation (NSF) [CBET-2053239]. The work done by Burgess Jr., Babushok and coworkers at National Institute of Standards and Technology (NIST) to develop chemical models for the combustion of HFC refrigerants greatly aided this study. We acknowledge the help of Elijah Levi for early work on the SRADIF model and Chin Ngai Mike Lam for extending the functionality of the pyMARS [40] library to perform kinetic model reduction using flame solutions. We would also like to thank Dr. Greg Linteris at NIST for

many fruitful discussions on various aspects of HFC combustion, and for generously providing us with raw experimental data, which was interpreted using SRADIF in SM-E.

6. Supplementary materials

Supplementary material associated with this article can be found, in the online version, at doi:…

7. References

[1] UNEP Ozone Secretariat. in Twenty-Eighth Meeting of the Parties to the Montreal Protocol on Substances that Deplete the Ozone Layer (Kigali, Rwanda, 2016); document UNEP/OzL.Pro.28/CRP/10, United Nations Environment Programme, (2016).

[2] K. Takizawa, K. Tokuhashi, S. Kondo, Flammability assessment of CH2=CFCF3: Comparison with fluoroalkenes and fluoroalkanes, J. Hazard. Mater. 172 (2009) 1329–1338.

[3] I. Bell, P. Domanski, G. Linteris, M.O. McLinden, Evaluation of binary and ternary refrigerant blends as replacements for R134a in an air-conditioning system (2018). 17th International Refrigeration and Air-Conditioning Conference at Purdue (2018), paper 1840.

[4] I. Bell, P. Domanski, G. Linteris, M.O. McLinden, The hunt for nonflammable refrigerant blends to replace R-134a, Int. J. Refrig. 104 (2019) 484-495.

[5] I. Bell, D. Riccardi, A. Bazyleva, M.O. McLinden, Survey of data and models for refrigerant mixtures containing halogenated olefins, J. Chem. Eng. Data 66 (2021) 2335-2354.

[6] M.O. McLinden, J.S. Brown, R. Brignoli, A.F. Kazakov, P.A. Domanski, Limited options for low-global-warming-potential refrigerants, Nat. Commun. 8 (2017) 1-9.

[7] G.T. Linteris, I.H. Bell, M.O. McLinden, An empirical model for refrigerant flammability based on molecular structure and thermodynamics, Int. J. Refrig. 104 (2019) 144-150.

[8] G. Linteris, V. Babushok, Laminar burning velocity predictions for C1 and C2 hydrofluorocarbon refrigerants with air, J. Fluor. Chem. 230 (2020) 109324.

[9] V.I. Babushok, D.R. Burgess Jr., D. Kim, M. Hegetschweiler, G.T. Linteris, Modeling of Combustion of Fluorine-Containing Refrigerants, NIST Technical Note 2170 (2021).

[10] K. Takizawa, A. Takahashi, K. Tokuhashi, S. Kondo, A. Sekiya, Burning velocity measurement of fluorinated compounds by the spherical-vessel method, Combust. Flame 141 (2005) 298-307

[11] P. Papas, S. Zhang, W. Kim, S.P. Zeppieri, M.B. Colket, P. Verma, Laminar flame speeds of 2,3,3,3-tetrafluoropropene mixtures, Proc. Combust. Inst. 36 (2017) 1145-1154.

[12] R.R. Burrell, G.T. Linteris, D.R. Burgess, M.J. Hegetschweiler, J.A. Manion, V. Babushok, R-152a/air and R-134a/oxygen constant volume spherical flame burning velocity measurements, 11th U. S. National Combustion Meeting, Pasadena, CA, (2019), paper 1f12.

[13] R.R. Burrell, J.L. Pagliaro, G.T. Linteris, Effects of stretch and thermal radiation on difluoromethane/air burning velocity measurements in constant volume spherically expanding flames, Proc. Combust. Inst. 37 (2019) 4231-4238.

[14] F.N. Egolfopoulos, N. Hansen, Y. Ju, K. Kohse-Höinghaus, C.K. Law, F. Qi, Advances and challenges in laminar flame experiments and implications for combustion chemistry, Prog. Energy Combust. Sci. 43 (2014) 36-67.

[15] K. Takizawa, S. Takagi, K. Tokuhashi, S. Kondo, M. Mamiya, and H. Nagai, Assessment of burning velocity test methods for mildly flammable refrigerants, Part 1: Closed-vessel method, ASHRAE Transactions 119 (2) (2013) 243-254.

[16] R. Hesse, L. Berger, C. Bariki, M.J Hegetschweiler, G.T Linteris, H. Pitsch, J. Beeckmann, Low global-warming-potential refrigerant CH2F2 (R-32): Integration of a radiation heat loss correction method to accurately determine experimental flame speed metrics, Proc. Combust. Inst. 38(3) (2021) 4665-4672.
[17] M.J. Hegetschweiler, J. Pagliaro, L. Berger, R. Hesse, J. Beeckmann, H. Pitsch, G. Linteris, Effects of stretch and radiation on the laminar burning velocity of R-32/air flames, Sci. Technol. Built Environ. 26(5) (2020) 599-609.
[18] B.C. Choi, J.S. Park, A.F. Ghoniem, Characteristics of outwardly propagating spherical flames of R134a(C2H2F4)/CH4/O2/N2 mixtures in a constant volume combustion chamber, Energy 95 (2016) 517-527.
[19] L. Berger, R. Hesse, K. Kleinheinz, M.J. Hegetschweiler, A. Attili, J. Beeckmann, G.T. Linteris, H. Pitsch, A DNS study of the impact of gravity on spherically expanding laminar premixed flames, Combust. Flame 216 (2020) 412-425.
[20] P.D. Ronney, H.Y. Wachman, Effect of gravity on laminar premixed gas combustion I: Flammability limits and burning velocities, Combust. Flame 62 (1985) 107-119.
[21] L. Qiao, Y. Gan, T. Nishiie, W.J.A. Dahm, E.S. Oran, Extinction of premixed methane/air flames in microgravity by diluents: Effects of radiation and Lewis number, Combust. Flame 157(8) (2010) 1446-1455.
[22] R. Hesse, C. Bariki, M.J. Hegetschweiler, G.T. Linteris, H. Pitsch, J. Beeckmann, Elucidating the challenges in extracting ultra-slow flame speeds in a closed vessel-A CH2F2 microgravity case study using optical and pressure-rise data, Proc. Combust. Inst. (2022) https://doi.org/10.1016/j.proci.2022.07.167.
[23] C.K. Law, F.N. Egolfopoulos, A unified chain-thermal theory of fundamental flammability limits, Symp. (Int.) Combust. 24(1) (1992) 137-144.
[24] Z. Chen, Effects of radiation and compression on propagating spherical flames of methane/air mixtures near the lean flammability limit, Combust. Flame 157 (2010) 2267-2276.
[25] Y. Ju, H. Guo, K. Maruta, F. Liu, On the extinction limit and flammability limit of non-adiabatic stretched methane–air premixed flames, J. Fluid Mech. 342 (1997) 315-334.
[26] J. Jayachandran, R. Zhao, F.N. Egolfopoulos, Determination of laminar flame speeds using stagnation and spherically expanding flames: Molecular transport and radiation effects, Combust. Flame 161 (2014) 2305-2316.
[27] J. Santner, F.M. Haas, Y. Ju, F.L. Dryer, Uncertainties in interpretation of high pressure spherical flame propagation rates due to thermal radiation, Combust. Flame 161 (2014) 147-153.
[28] Y. Ju, G. Masuya, P.D. Ronney, Effects of radiative emission and absorption on the propagation and extinction of premixed gas flames, Proc. Combust. Inst. 27(2) (1998) 2619-2626.
[29] H. Yu, W. Han, J. Santner, X. Gou, C.H. Sohn, Y. Ju, Z. Chen, Radiation-induced uncertainty in laminar flame speed measured from propagating spherical flames, Combust. Flame 161 (2014) 2815-2824.
[30] S.H. Sohrab, C.K. Law, Extinctions of premixed flames by stretch and radiative loss, Int. J. Heat Mass Transf. 27(2) (1984) 291-300
[31] H. Nakamura, M. Shindo, Effects of radiation heat loss on laminar premixed ammonia/air flames, Proc. Combust. Inst. 37 (2019) 1741-1748.
[32] M.J. Hegetschweiler, J.L. Pagliaro, L. Berger, R. Hesse, J. Beeckmann, C. Bariki, H. Pitsch, G.T. Linteris, Data reduction considerations for spherical R-32(CH2F2)-air flame experiments, Combust. Flame 237 (2022) 111806.
[33] D.R. Burgess Jr., R.R. Burrell, V.I. Babushok, J.A. Manion, M.J. Hegetschweiler, G.T. Linteris, Burning velocities of R-32/O2/N2 mixtures: Experimental measurements and development of a validated detailed chemical kinetic model, Combust. Flame 236 (2022).

[34] C. Xiouris, T. Ye, J. Jayachandran, F.N. Egolfopoulos, Laminar flame speeds under engine-relevant conditions: Uncertainty quantification and minimization in spherically expanding flame experiments, Combust. Flame 163 (2016) 270-283.
[35] M. Faghih, Z. Chen, The constant-volume propagating spherical flame method for laminar flame speed measurement, Sci. Bull. 61(16) (2016) 1296-1310.
[36] D.G. Goodwin, R.L. Speth, H.K. Moffat, B.W. Weber, Cantera: An object-oriented software toolkit for chemical kinetics, thermodynamics, and transport processes. https://www.cantera.org, 2021. Version 2.5.0.
[37] C. Womeldorf, W. Grosshandler, Flame extinction limits in CH2F2/air mixtures, Combust. Flame 118(1-2) (1999) 25-36.
[38] V.I. Babushok, D.R. Burgess Jr., M.J. Hegetschweiler, G.T. Linteris, Flame propagation in the mixtures of O2/N2 oxidizer with fluorinated propene refrigerants (CH2CFCF3, CHFCHCF3, CH2CHCF3), Combust. Sci. Technol. 193 (2021) 1949-1972.
[39] V.I. Babushok, D.R. Burgess Jr, D.K. Kim, M.J. Hegetschweiler, G.T. Linteris, Modeling of Combustion of Fluorine-Containing Refrigerants, NIST Technical Note TN 2170 (2021).
[40] P.O. Mestas, P. Clayton, and K.E. Niemeyer. (2019) pyMARS v1.1.0 [software].
[41] S.P Fuss, A. Hamins, Determination of Planck mean absorption coefficients for HBr, HCl, and HF, J. Heat Transf. 124(1) (2002) 26-29.
[42] F. Takahashi, V.R. Katta, G.T. Linteris, V.I. Babushok, Combustion inhibition and enhancement of cup-burner flames by CF3Br, C2HF5, C2HF3Cl2, and C3H2F3Br, Proc. Combust. Inst. 35 (2015) 2741-2748.
[43] A.P. Modica, R.R. Brochu, COF2 Band Intensities in the 2.0 ~ 6.0 Micron Region, J. Quant. Spectrosc. Radiat. Transfer 9 (1969) 1105-1116.
[44] R. Lawson, V. Gururajan, A. Movaghar, F.N. Egolfopoulos, Autoignition of reacting mixtures at engine-relevant conditions using confined spherically expanding flames, Proc. Combust. Inst. 38 (2021) 2285-2293.
[45] D. Bradley, P.H. Gaskell, X.J. Gu, Burning velocities, Markstein lengths, and flame quenching for spherical methane-air flames: A computational study, Combust. Flame 104(1-2) (1996) 176-198.
[46] H. Wu, P.C. Ma, M. Ihme, Efficient time-stepping techniques for simulating turbulent reactive flows with stiff chemistry, Comput. Phys. Commun. 243 (2019) 81-96.
[47] C.D. Needham, P.R. Westmoreland, Combustion and flammability chemistry for the refrigerant HFO-1234yf (2,3,3,3-tetrafluoropropene), Combust. Flame 184 (2017) 176-185
[48] M.R. Zachariah, W. Tsang, P.R. Westmoreland, D.R.F. Burgess Jr., Theoretical prediction of the thermochemistry and kinetics of reactions of CF_2O with hydrogen atom and water, J. Phys. Chem. 99 (1995) 12512-12519.